Structural Engineering and Mechanics, Vol. 44, No. 6 (2012) 801-814
DOI: http://dx.doi.org/10.12989/sem.2012.44.6.801

Strain-rate effects on interaction between Mode I matrix crack and inclined elliptic inclusion under dynamic loadings

Ying Li, Wan-Chao Qiu, Zhuo-Cheng Ou*, Zhuo-Ping Duan and Feng-Lei Huang

State Key Laboratory of Explosion Science and Technology, Beijing Institute of Technology, Beijing 100081, China

(Received February 29, 2012, Revised September 1, 2012, Accepted November 8, 2012)

Abstract. The strain rate effects on the interaction between a Mode I matrix crack and an inclined elliptic matrix-inclusion interface under dynamic tensile loadings were investigated numerically, and the results are in agreement with previous experimental data. It is found, for a given material system, that there are the first and the second critical strain rates, by which three kinds of the subsequent crack growth patterns can be classified in turn with the increasing strain rate, namely, the crack deflection, the double crack mode and the perpendicular crack penetration. Moreover, such a crack deflection/penetration behavior is found to be dependent on the relative interfacial strength, the inclined angle and the inclusion size. In addition, it is shown that the so-called strain rate effect on the dynamic strength of granule composites can be induced directly from the structural dynamic response of materials, not be entirely an intrinsic material property.

Keywords: cohesive crack; dynamic strength; strain rate effects; crack propagation; crack penetration; composites

1. Introduction

Granule composites have been extensively used in practical engineering applications due to their excellent combinatorial properties, especially in the field of military and civilian facilities, protecting from possible impact loadings resulted for example from the earthquake wave, high-velocity impacting and explosion shock waves, such as airport runways, the protective shells of nuclear fuel in nuclear power plants, the protective armors of tanks and warships, and so on. However, the internal microcracks inside any phase of granule composites will seriously influence the overall mechanical properties even the fracture behaviors, especially under dynamic loadings, and hence it is of significance to understand in depth the failure behaviors of composite materials under dynamic loadings.

Generally, a granule composite such as concrete can be taken as a three-phase material composed of the matrix, inclusions and matrix-inclusion interfaces, which makes the mechanism of the microcrack propagation and material failure very complicated. Moreover, it is believed that the

*Corresponding author, Professor, E-mail: zcou@bit.edu.cn

microcrack growths and failure modes in a granule composite under dynamic loadings are different remarkably from that under quasistatic one because of the material inertia. For instance, via Split Hopkinson Press Bar technique, Brara and Klepaczko (2007) investigated experimentally the fracture energy of concrete under dynamic tensile loadings and observed that most of the aggregates are ruptured under higher loading rates, but remain intact by and large under a relative lower one. In other words, high-rate dynamic loadings can result in more inclusion failure, but, in contrast, the interfacial fracture is dominant under relative lower strain rate, which is obviously dependent on the energy redistribution when a matrix crack encounters a matrix-inclusion interface. On the other hand, as reviewed recently by Cotsovos and Pavlović (2008) from a great number of previous dynamic tensile and compressive experimental data, the dynamic strength of concrete material increases considerably under high-rate loadings, which is usually called as the strain-rate effects on material strength. Moreover, for a certain material, it seems that there exists a critical transition strain rate ($\sim 10^2 \sim 10^3\,s^{-1}$), above which the strength increase with the strain rate becomes much faster. Similar features are also founded in other granule composites (Cai *et al.* 2007, Wei and Hao 2009). In the opinion of authors of this paper, physically, such a transition strain rate should imply some critical phenomenon, in which the inclusion fracture under high-rate dynamic loadings may play an important role, because that in general the strength of the inclusions in a composite is much higher than that of both the matrix and the matrix-inclusion interface and then much more energy will be dissipated for the inclusion fracture.

The aim of this paper is therefore to investigate in more detail the strain rate effects on the interaction between a matrix crack and an elliptic inclusion. By using the ABAQUS software together with a bilinear Cohesive Zone Model, the strain rate effect and some predominating influence factors such as relative interfacial strength, the inclined angle and the local curvature of the interface at the crack as well as the sizes of the inclusion are simulated numerically. The organization of this paper is as follows: In Section 2, the governing equation including the bilinear Cohesive Zone Model and the finite element model are described briefly, and the numerical finite element is introduced in Section 3. The computational results associated with some discussions are then presented in Section 4, and, finally, some conclusions are drawn out in Section 5.

2. Governing equations and finite element model

For the integrality as well as the readability, the governing equations treated numerically in this study are presented briefly. According to the continuum mechanics, the particle displacement vector $\mathbf{u}$ and the deformation gradient tensor $\mathbf{F}$ can be written, respectively, as

$$\mathbf{u} = \mathbf{x} - \mathbf{X}, \quad \mathbf{F} = \frac{\partial \mathbf{x}}{\partial \mathbf{X}} \tag{1}$$

where $\mathbf{x}$ and $\mathbf{X}$ are the Eulerian and the Lagrangian coordinates, respectively. In the reference configuration, the governing equation in the absence of the body force can be written in the form of the principle of virtual work as following (Siegmund *et al.* 1997)

$$\int_V \boldsymbol{\sigma} : \delta\mathbf{F}\, dV - \int_{S_{int}} \mathbf{T} \cdot \delta\mathbf{u}\, dS = \int_{S_{ext}} \mathbf{T} \cdot \delta\mathbf{u}\, dS - \int_V \rho \frac{\partial^2 \mathbf{u}}{\partial t^2} \cdot \delta\mathbf{u}\, dV \tag{2}$$

where σ is the nominal Cauchy stress tensor; V, Sext and Sint are the volume, external and internal surface areas, respectively, of the considered block, and $T = \sigma \cdot n$ is the traction vector acted on the surfaces with a normal n. In the absence of the body force, Eq. (2) can then be expressed as following componentwise form in the two dimensional Lagrangian coordinate system

$$\begin{cases} \rho \dfrac{\partial^2 u_X}{\partial t^2} = \dfrac{\partial \sigma_{XX}}{\partial X} + \dfrac{\partial \sigma_{YX}}{\partial Y} \\ \rho \dfrac{\partial^2 u_Y}{\partial t^2} = \dfrac{\partial \sigma_{XY}}{\partial X} + \dfrac{\partial \sigma_{YY}}{\partial Y} \end{cases} \tag{3}$$

where u_X and u_Y are the components of the displacement vector **u** in the X and Y axes, respectively, and t is the time variable.

To deal with such an issue on interfacial cracks, two kinds of constitutive models are adopted for different material behaviors in different computational zones. One is the linear elastic Hooke law, which is used to describe the mechanical properties of the matrix as well as the inclusion materials; the other is the so-called Cohesive Zone Model (CZM) used to describe the possible crack growth. The cohesive zone model was initially proposed by Barenblatt (1959) and Dugdale (1960) independently to eliminate the crack-tip stress singularity in brittle materials. Since the pioneer work, a number of different kinds of CZM (Rice and Wang 1989, Needleman 1990a, Tvergaard 1990, Xu and Needleman 1993, Tvergaard and Hutchinson 1992, Camacho and Ortiz 1996, Geubelle and Baylor 1998) have been developed such as the quadratic (Rice and Wang 1989), the exponential (Xu and Needleman 1993) and the bilinear models (Geubelle and Baylor 1998). In this paper, the bilinear CZM is adopted in the following form

For $\Delta_n > 0$

$$T_n = \begin{cases} \dfrac{T_{n\max}}{\Delta_n^*}\Delta_n & (\Delta_n \le \Delta_n^*) \\ \dfrac{T_{n\max}}{\Delta_{n\max} - \Delta_n^*}(\Delta_{n\max} - \Delta_n) & (\Delta_n^* < \Delta_n \le \Delta_{n\max}) \end{cases} \tag{4}$$

$$T_t = \begin{cases} \dfrac{T_{t\max}}{\Delta_t^*}\Delta_t & (\Delta_t \le \Delta_t^*) \\ \dfrac{T_{t\max}}{\Delta_{t\max} - \Delta_t^*}(\Delta_{t\max} - \Delta_t) & (\Delta_t^* < \Delta_t \le \Delta_{t\max}) \end{cases} \tag{5}$$

For $\Delta_n = 0$

$$T_t = \begin{cases} \dfrac{T_{t\max}}{\Delta_t^*}\Delta_t & (\Delta_t \le \Delta_t^*) \\ \dfrac{T_{t\max}}{\Delta_{t\max} - \Delta_t^*}(\Delta_{t\max} - \Delta_t) & (\Delta_t^* < \Delta_t \le \Delta_{t\max}) \end{cases} \tag{6}$$

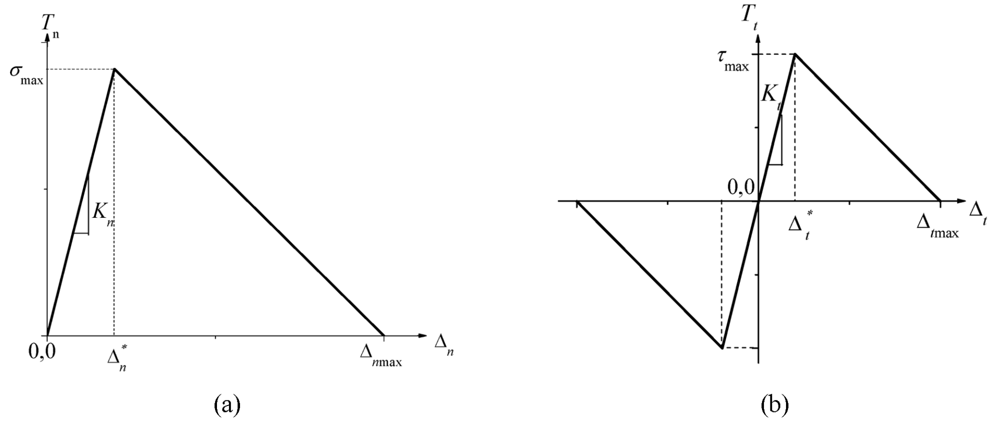

Fig. 1 (a) Cohesive zone model for Mode I crack, (b) Cohesive zone model for Mode II crack

where Δ_n and Δ_t denote, respectively, the normal and tangential separations between the upper and the lower surfaces of the cohesive elements with the critical values of $\Delta_{n\max}$ and $\Delta_{t\max}$; Δ_n^* and Δ_t^* are the normal and the tangential characteristic length parameters of the interface, respectively; T_n and T_t are the normal and tangential components, respectively, of the traction vector $\mathbf{T}$ with corresponding maximum interfacial load-carrying stress $T_{n\max}$ and $T_{t\max}$ characterizing the initiation of the subsequent material soften process. As an example, the variation of normal and tangential tractions with respect to Δ_n and Δ_t in the cases of the pure opening ($\Delta_t = 0$) and the pure shear separation ($\Delta_n = 0$), respectively, are shown in Fig. 1. Moreover, the normal (G_{IC}) and tangential (G_{IIC}) works of separation per unit area of interface needed to complete the crack-tip opening (i.e., the total area under the constitutive curve) are given, respectively, by

$$G_{IC} = \frac{1}{2}\Delta_{n\max}T_{n\max}, \quad G_{IIC} = \frac{1}{2}\Delta_{t\max}T_{t\max} \tag{7}$$

Generally, under the pure tensile or the pure shear stress, the material damage is assumed to initiate only when certain critical stresses have been reached. However, under the mixed-mode loadings, the damage initiation can usually occur when both of the normal and the tangential tractions are below each of their critical values. Therefore, the quadratic failure criterion (Buyukozturk and Hearing 1998) to predict the initiation of the softening process under mixed-mode loadings is adopted as

$$\left(\frac{T_n}{T_{n\max}}\right)^2 + \left(\frac{T_t}{T_{t\max}}\right)^2 = 1 \tag{8}$$

Moreover, to predicate the complete opening of a mixed-mode cohesive crack, the B-K fracture criterion proposed by Benzeggagh and Kenane (1996) is used, which is expressed as

$$G = G_C \tag{9}$$

where

$$G_C = G_{IC} + (G_{IIC} - G_{IC})\left(\frac{G_I}{G_I + G_{II}}\right)^{\eta} \tag{10}$$

where G_I and G_{II} are energy release rates of Mode I and II cracks, respectively, or the normal and tangential works of separation per unit area of the interface, and the parameter η can be obtained from the mixed mode bending (MMB) tests at different mode ratios.

It should be pointed out here that some researchers believe that the normal cohesive traction should decrease when tangential separation increases because the increase of the tangential separation leads to material damage, and thus the reduction of resisting capacity is expected. However, on the one hand, up to now, how does the normal cohesive traction decrease with the tangential separation is not understood very well, and, on the other hand, such an influence can be compensated partly by the mixed failure criterion of Eq. (8). Moreover, it has also been noticed in our numerical computation that the decrease of the normal cohesive traction with the increasing tangential separation is always not so high, which can then be ignored reasonably.

3. Computational finite element model

Under the two-dimensional plane strain condition, in the numerical simulation, an initial Cartesian reference coordinate frame is used, with its origin designed at the crack tip, and the computational domain is depicted in Fig. 2. An inclined elliptic inclusion with its semi-major axis a and semi-minor axis b is embedded in a rectangle region occupied by the matrix material with the length and the width of L = 20.0 mm and W = 12.0 mm, respectively. A semi-infinite-like horizontal matrix crack with l = 5.0 mm in length is assumed to be terminated at an end point of the minor axis on the matrix-inclusion interface, and the angle between the initial crack and the minor axis of the elliptic interface is denoted by θ.

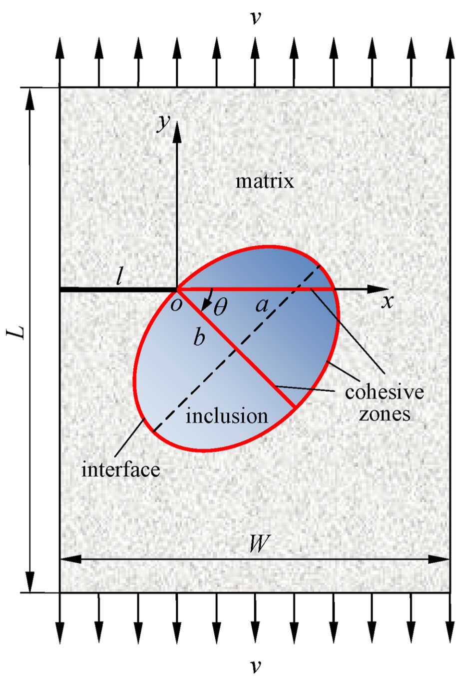

Fig. 2 Computational domain

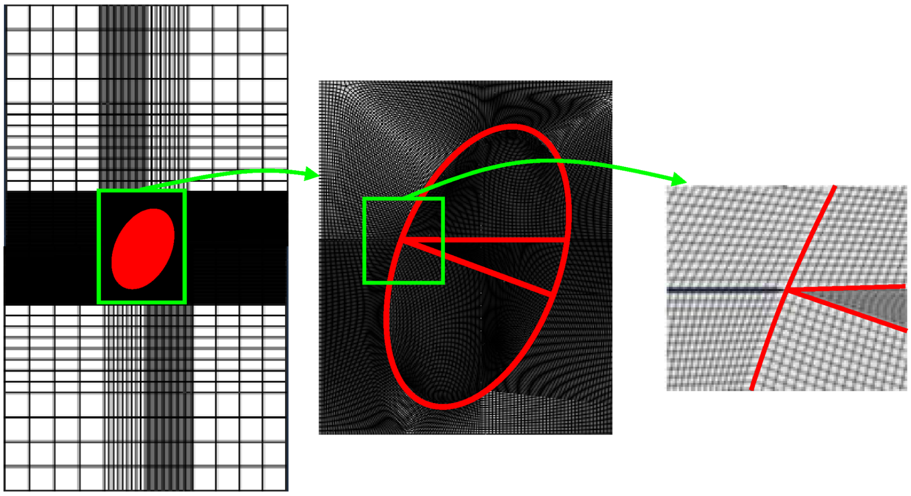

Fig. 3 Finite element meshes

Certainly, there exist an infinite number of possible crack growth paths or directions after the crack deflection/penetration. However, for the sake of simplicity, only three extreme crack growth paths are investigated in the study (i.e., the interfacial crack growth direction, the self-similar crack growth direction and that perpendicular to the matrix-inclusion interface) to avoid some intrinsic difficulties in the numerical simulation under the assumption of multi-crack growth paths, such as the strong elements coupling and the change of the global material property of the inclusion, which have not been fixed well up to now.

In the numerical computations, the quadrilateral bulk elements are adopted as shown in Fig. 3. To save the computational time, the uniform region in the inclusion and the initial crack tip are surrounded by gradual enlarged meshes out to the specimen boundaries. The elements' sides used in the uniform region are about 20 μm in length. Generally, as proposed by Zhang and Paulino (2005), the length of the crack process zone should be about five times greater than that of the cohesive elements to ensure the computational convergence. According to Rice (1968), the cohesive zone can be estimated approximately by

$$l = \frac{\pi}{8}\frac{E}{1-\upsilon^2}\frac{G_{IC}}{T_{avg}^2} \tag{11}$$

which reaches a cohesive zone length of 121.1 μm for the materials used in the study, and thus the computational convergence can be ensured. In fact, some trial numerical computations were carried out using different elements' sides such as 10, 15 and 20 μm, which all reach the same numerical results within a good precision.

The constitutive properties of both the matrix and the inclusion are assumed to be linear elastic and thus can be described by corresponding Hooke's law. The material parameters used in the study are listed in Table 1 (Zhang and Paulino 2005), in which E, ν and ρ are the Young modulus, Poisson ratio and mass density, respectively. On the other hand, the crack growth is described by the above mentioned bilinear CZM. To allay as could as possible the influence of the CZM on the original material properties, only three pieces of zero-thickness cohesive elements are inserted along the possible crack growth directions, i.e., along the interface as well as the direction of the self-

Table 1 Material properties

	E (GPa)	ν	ρ (g/mm^3)
Matrix	27.8	0.2	1.5
Inclusion	42.2	0.16	2.8

Table 2 Cohesive element parameters

Material	$G_{IC} = 0.5G_{IIC}$ (N/m)	k_n (N/mm^3)	k_t (N/mm^3)	$T_{n\max}$ (MPa)	$T_{t\max}$ (MPa)	η
Interface		10^7	3×10^7			2.2
Inclusion	50. 04	1.5×10^7	4.5×10^7	185.0	555.0	2.2

similar crack growth and of that perpendicular to the interface inside the inclusion. The cohesive parameters used are listed in Table 2 (Rice 1968).

As for the boundary condition, the external loadings in the form of velocity are assumed to act on both of the upper and lower surfaces, which are written as

$$v(X_1, X_2 = \pm L, t) = \bar{v}(\xi) = \begin{cases} \gamma\xi & 0 < \xi \le \xi_r \\ \gamma\xi_r = v_0 & \xi > \xi_r \end{cases} \tag{12}$$

where v denotes the particle velocity; $\bar{v}$ means the boundary velocity loading; t is the time variable and ξ denotes the local time argument, reckoned from the time when the stress wave arrives just at the considered location, with the loading rising time ξ_r; γ is a constant, which can be used as a measure of the loading rate, and v_0 is the loading amplitude. Additionally, the whole computational system is assumed to be initial static and free of stresses.

4. Results and discussions

The numerical simulation was performed by using the ABAQUS applied software. To understand comprehensively the competition between the crack deflection and penetration under dynamic loadings, some kinds of predominating factor including the loading rate (or the strain rate $\dot{\varepsilon}$), the relative interfacial strength (represented by the relative fracture toughness $G_C^{(int)}/G_C^{(2)}$), the inclined angle θ of the interface related to the initial crack and the inclusion size (represented in this study by the local radius of curvature of interface R at the crack tip and the area of inclusion S) were taken into account. Hereinafter, the superscripts "(int)" and "(2)" are taken to represent the variables corresponding to the interface and the inclusion, respectively, unless other demonstrations. In the following, the numerical results and some discussions are presented.

Firstly, the numerical results on the crack deflection/penetration behaviors under different strain rates ($\dot{\varepsilon} = 300\ \mathrm{s}^{-1}, 500\ \mathrm{s}^{-1}, 800\ \mathrm{s}^{-1}$) are presented as shown respectively in Figs. 4(a)-4(c), where the relative interfacial strength of $G_C^{(int)}/G_C^{(2)} = 0.49$, the inclined angle of $\theta = 20^\circ$ and the semi-major and semi-minor axis of a = 1.8 mm and b = 1.0 mm, respectively, are assumed. It can be seen from Fig. 4 that, under a relatively lower strain-rate such as $\dot{\varepsilon} = 300\ \mathrm{s}^{-1}$, the initial matrix crack deflects into and propagates along the interface, as shown in Fig. 4(a); while, under a

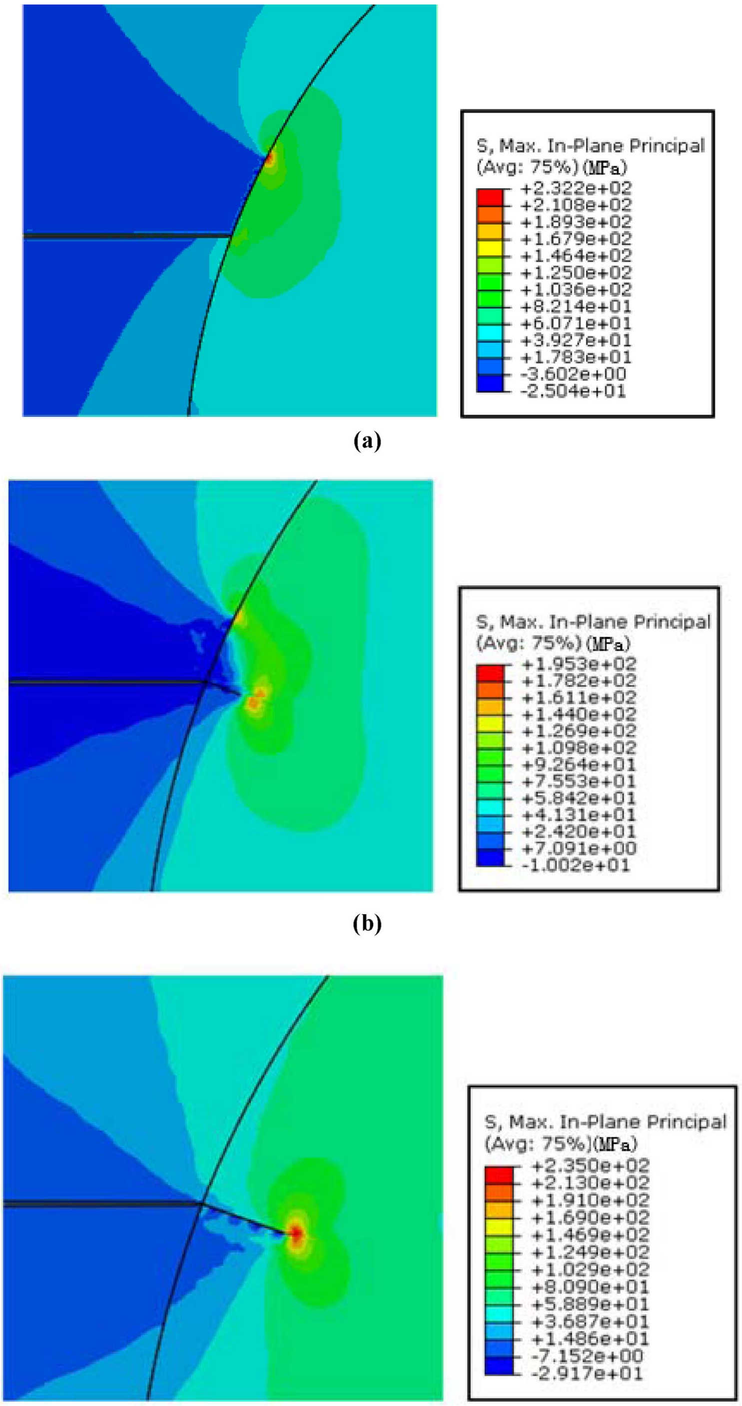

(c)

Fig. 4 Contours of maximum principal effective stress and crack location. $G_C^{(int)}/G_C^{(2)} = 0.49$, $t = 32\ \mu$s, (a) $\dot{\varepsilon} = 300\ \mathrm{s}^{-1}$, (b) $\dot{\varepsilon} = 500\ \mathrm{s}^{-1}$, (c) $\dot{\varepsilon} = 800\ \mathrm{s}^{-1}$

relatively higher strain-rate of $\dot{\varepsilon} = 500\ \mathrm{s}^{-1}$, beside the deflected crack, another crack is initiated subsequently, which penetrates across the interface and propagates along the direction perpendicular to the interface, as shown in Fig. 4(b), and this can be termed as a double-crack mode; moreover, when the strain-rate reaches up to $\dot{\varepsilon} = 800\ \mathrm{s}^{-1}$, see Fig. 4(c), the initial matrix crack will penetrate directly across the interface and propagates along the direction perpendicular to the interface, without any deflection at all. That is to say, under dynamic loadings, there exists two critical strain rates which are called here the first critical strain rate ($\dot{\varepsilon}_{crit}^{(1)}$) and the second critical strain rate ($\dot{\varepsilon}_{crit}^{(2)}$). The crack deflection/penetration behaviors under dynamic loadings can then be divided into three crack growth mode, namely, the crack deflection when $\dot{\varepsilon} < \dot{\varepsilon}_{crit}^{(1)}$, the double crack mode when $\dot{\varepsilon}_{crit}^{(1)} < \dot{\varepsilon} < \dot{\varepsilon}_{crit}^{(2)}$ and the perpendicular crack penetration when $\dot{\varepsilon} > \dot{\varepsilon}_{crit}^{(2)}$. By the way, it is also found that, for an interface strong enough such as that with $G_C^{(int)}/G_C^{(2)}$ greater than about 0.6, there exists the self-similar crack penetration (i.e., the crack penetrates the interface and propagates along the self-similar growth direction) under higher strain rates. However, such a high strength interface can hardly be encountered in practical engineering applications, and hence the self-similar crack penetration is not considered in the study.

As is well known, a crack in a homogeneous material usually propagates along its self-similar growth direction when a certain fracture criterion is satisfied. However, when a matrix crack approaches to and encounters a bimaterial interface, several subsequent crack growth paths can be expected such as the crack deflection and the crack penetration. This is resulted from the redistribution of fracture energy and depends on both the loading conditions and the physical properties of both the matrix and the inclusion as well as of the bimaterial interface, or, in other words, the crack will propagate in the direction along which the fracture criterion has been satisfied at first. In general, under quasistatic loadings or lower strain-rate, the matrix crack deflects into and propagates along the interface if the relative interfacial strength is lower, due to that the fracture toughness of a bimaterial interface in composite materials is usually much lower than that of the inclusions and that there is enough time to complete the fracture energy redistribution. With the increase of the strain rate, the fracture energy contributed to the crack penetration will increase gradually, which makes occurrence of the double crack mode when the strain rate reaches up to the first critical strain rate $\dot{\varepsilon}_{crit}^{(1)}$. Moreover, for higher strain rates that greater than the second critical strain rate $\dot{\varepsilon}_{crit}^{(2)}$, the crack penetration is realized, which implies that there is almost no time for the fracture energy to be redistributed and hence no enough fracture energy can be contributed to the interface failure. In addition, it is believed that the perpendicular rather than the self-similar crack penetration is resulted from the inclined interface, which makes the mixed-mode crack growth a dominating fracture mode. This, however, should be investigated in more detail in future. The above described results are in agreement with previous experimental observations. In fact, by an experimental investigation for concrete, Brara and Klepaczko (2007) has observed that the number of fractured aggregates increases obviously with the strain rate. On the other hand, it is worthy of noticing the direct inference of the above mentioned results that the total fracture energy, or, in other words, the dynamic strength of a composite material should be increase with the strain rate, because that failure of the inclusions will dissipate much more energy than that of the bimaterial interfaces. In fact, as reviewed by Cotsovos and Pavlović (2008), previous experimental data on concrete shows that there indeed exists a certain critical strain rate, over which a sudden increase of the dynamic material strength can be expected. In addition, we emphasize here that the above obtained results also show that failure of the inclusions under high strain rates is a dominating underlying mechanism of the so-called strain rate effect on the dynamic strength of composite materials,

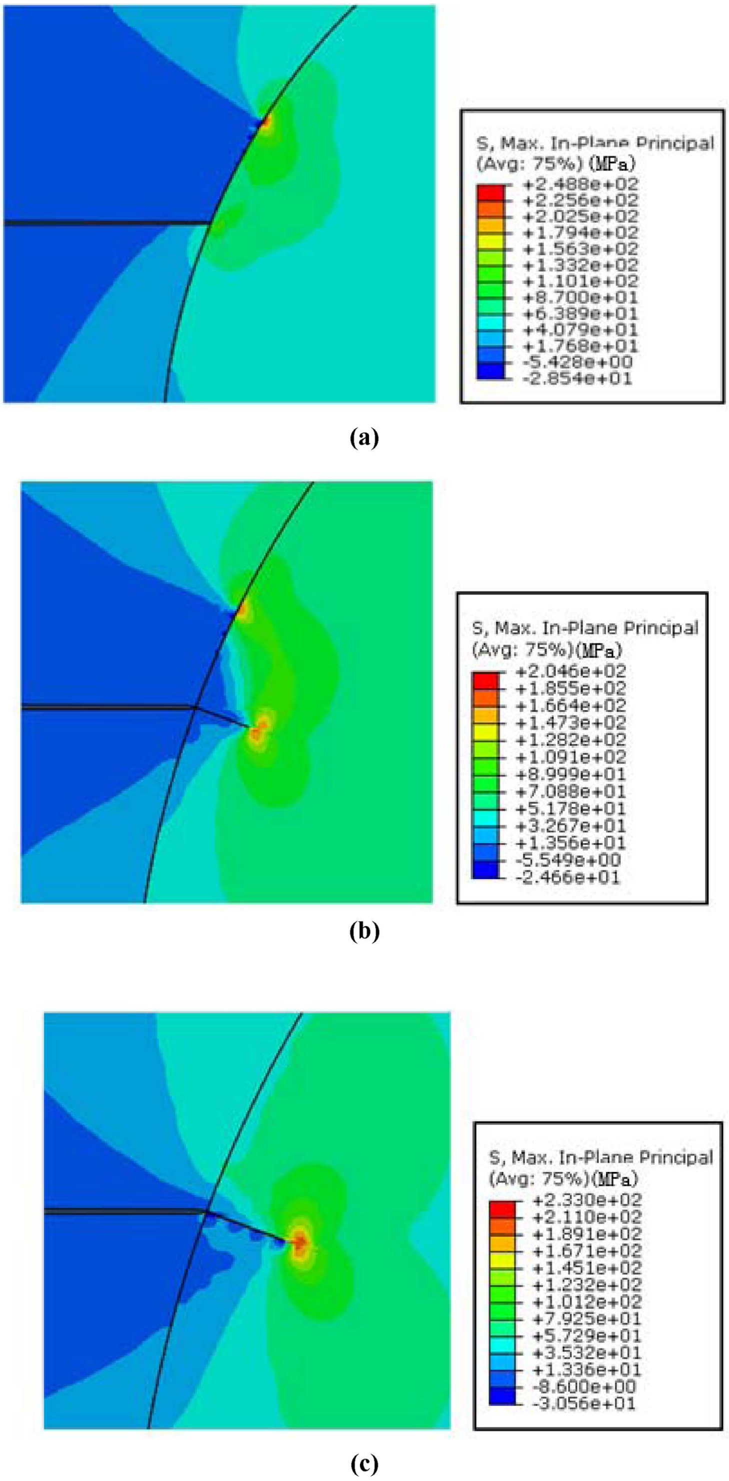

Fig. 5 Contours of maximum principal effective stress and crack location. $\dot{\varepsilon} = 856\ \mathrm{s}^{-1}$, $t = 32\ \mu\mathrm{s}$, (a) $G_C^{(int)}/G_C^{(2)} = 0.48$, (b) $G_C^{(int)}/G_C^{(2)} = 0.49$, (c) $G_C^{(int)}/G_C^{(2)} = 0.50$

considering that all the material parameters used in the computation are quasi-static one. This, furthermore, implies that the strain-rate effect on the strength of a composite material is dependent on the material inertia as well as on the boundary loading conditions and thus not an intrinsic material properties, which has been noticed recently by some authors (Liu *et al*. 2010, Ou *et al*. 2010) of this paper and other investigators (Klepaczko and Brara 2001, Weerheijm and Van Doormaal 2007).

Next, the effect of the interfacial strength on the crack deflection/penetration behavior has been investigated. For a certain strain rate ($\dot{\varepsilon}$ = 500 s^{-1}) and the same geometric conditions of the computational configuration as described above, the numerical results on the crack deflection/penetration for different relative interfacial strengths of ($G_C^{(int)}/G_C^{(2)}$ = 0.48, 0.49, 0.50) are presented in Figs. 5(a)-5(c). It can be observed that the crack deflection, the double-crack mode and the perpendicular crack penetration occur in turn with increase of the relative interfacial strength, implying that higher interfacial strengths is propitious to the crack penetration. Such a crack deflection/penetration behavior seems harmonious to the analytical results presented by He and Hutchinson (He and Hutchinson 1989) under the quasi-static loadings. Moreover, similarly to the existence of the critical strain rates, there are two critical interfacial strengths under a certain strain-rate, by which the crack deflection/penetration can also be divided in turn into the crack deflection, the double-crack mode and the perpendicular crack penetration with the increasing relative interfacial strength.

Thirdly, the influence of the inclined angle θ on the crack deflection/penetration behaviors is also investigated under the same geometric configuration. Fig. 6 shows the relationship between the relative interfacial strength and the critical strain rates for the different inclined angles of θ = 15° and θ = 20°. It is seen that both the critical strain rates and the critical relative interfacial strengths increase with the inclined angle, which is in agreement with previous experimental results (Qi *et al*. 1989). In other words, the crack penetration becomes more difficult with the increase of the inclined angle.

Finally, the influence of the inclusion size on the crack deflection/penetration behavior is

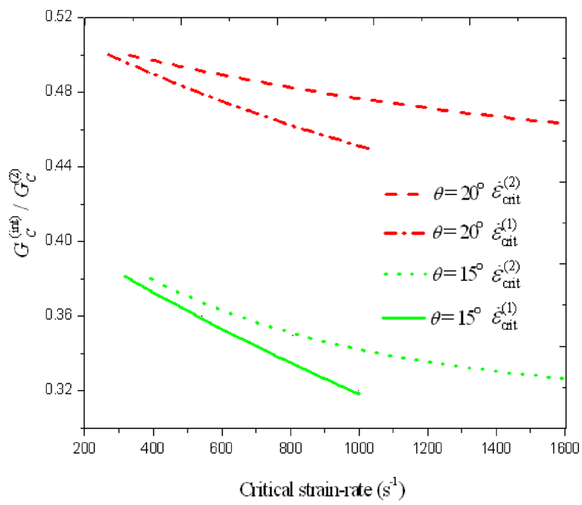

Fig. 6 Relationship between critical strain-rates and interfacial strength under constant local curvature of interface and inclusion sizes

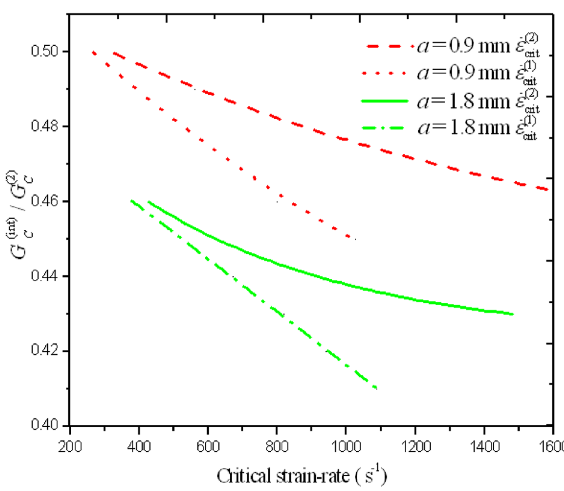

Fig. 7 Relationship between the critical strain-rate and the interfacial strength under the constant ratio *a/b* and interfacial inclined angle

investigated. The numerical results for the relation curve between the critical strain-rate and the relative interfacial strength for two given inclusion sizes (a = 1.8 and 0.9 mm under a/b = 2.0) under a constant inclined angle of $\theta = 20^{\circ}$ are presented as shown in Fig. 7. It can be seen, for a certain interfacial strength, the critical strain-rates decrease with the size of inclusion, which implies that the larger the size of inclusion is, the easier the crack penetration occurs. Moreover, it should be noticed, under the similar transformation of the size of elliptical inclusion for a constant ratio of the semi-major to the semi-minor axis a/b, that the inclusion area (in a two dimensional sense) and the local curvature of interface at the crack-tip are different, and their influences on the crack deflection/penetration behaviors can also be investigated. On the one hand, the influence of different local curvatures of the interface at the crack tips (R = 3.24 mm with a = 1.8 mm and b = 1.0 mm; R = 1.34 mm with $a = b =$ 1.34 mm) on the crack deflection/penetration behaviors under a certain inclined angle of $\theta = 20^{\circ}$ with a fixed area of inclusion (S = 5.652 mm^2) is studied, and the numerical results are depicted as shown in Fig. 8. It is found that the larger the local radius of curvature is, the easier the crack penetration occurs. Physically, a smaller radius of curvature makes the energy turning to the interface easier, and then higher critical strain rates are required for the crack penetration. On the other hand, taking a constant local radius of curvature (R = 1.62 mm) and inclined angle ($\theta = 20^{\circ}$), the numerical results for the relationship between the critical strain rates and the interfacial strength under different inclusion areas (S = 1.413 mm^2 with a = 0.9 mm and b = 0.5 mm, S = 8.24 mm^2 with $a = b$ = 1.62 mm) are obtained and depicted in Fig. 9. It is very interesting to notice that all the computational results under different inclusion areas can be fitted into just one curve with a good precision, and hence a universal relationship may be implied. In other words, the influence of inclusion sizes on the strain-rate effects on the crack deflection/ penetration can then be characterized only by that of the local curvature of the interface at the crack tip. In fact, such a local characteristic is also consistence with the concept of wave, in which all the dynamic response can be determined by the local properties in a neighborhood near the point under consideration, and the higher the strain-rate, the smaller the neighborhood.

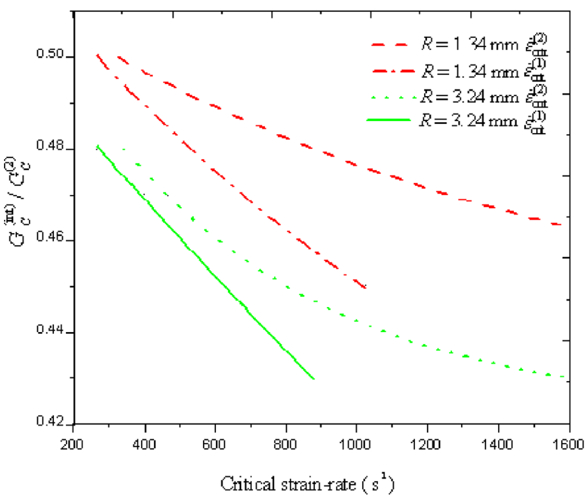

Fig. 8 Relationship between critical strain-rates and interfacial strength under constant inclined angle of interface and inclusion areas

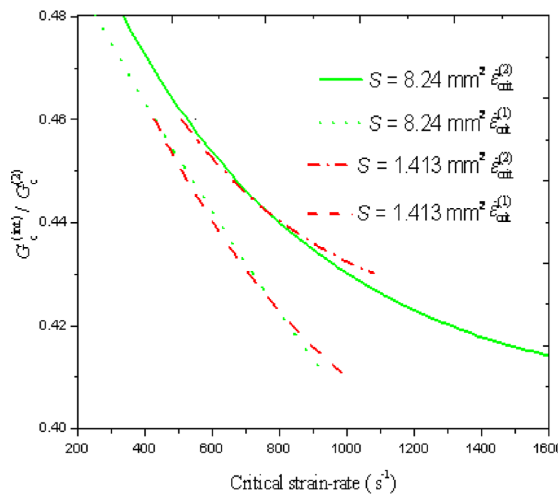

Fig. 9 Relation between critical strain rates and interfacial strength under constant inclined angle and local curvature of interface

5. Conclusions

The strain-rate effects on the interaction between a Model I matrix crack and an inclined elliptic matrix-inclusion interface under dynamic loadings are investigated numerically by using the ABAQUS applied software, together with the bilinear CZM. It is found that the loading rate (or the strain-rate), the relative interfacial strength, the inclined angle and the size of the inclusion all can affect markedly the crack deflection/penetration behaviours, and following conclusions can be drawn out.

At first, for a certain relative interfacial strength, there exist the first and the second critical strain rates, by which three kinds of subsequent crack growth patterns can be classified in turn with the increasing strain rate, namely, the crack deflection, the double-crack mode and the perpendicular crack penetration, and then we demonstrate that the experimental observed critical transition strain rate for the sudden increase of the strain rate effect on the strength of granule composite materials such as concrete is resulted from failure of the inclusions. Moreover, the strain-rate effects on the dynamic strength of granule composites can be induced directly by such a structural dynamic response of materials because of inertia effects, which implies that the so-called strain rate effect should not be entirely an intrinsic material property. Next, the competition between the crack deflection and penetration under dynamic loadings is dependent remarkably on the relative interfacial strength. That is, in principle, a higher relative interfacial strength is always propitious to the crack penetration, and thus the good matrix-inclusion interfaces can increase the dynamic strength of a granule composite material such as concrete, which is also consistent qualitatively with previous experimental data (Brara and Klepaczko 2007). Thirdly, it is also found that a larger inclined angle of the interface at the crack tip can conduce to the crack deflection. Finally, the influence of the inclusion size on the crack deflection/penetration is also taken into account, and it is found that, the critical strain-rate is dependent only on the local curvature of interface at the crack-tip, regardless of the sizes and shape of the inclusion, and both the critical strain rates and the critical relative interfacial strengths decrease with the local curvature radius of the interface.

Acknowledgements

This paper is supported by the National Science Foundation of China (No. 10872035) and the Foundation of Key State Laboratory of Explosion Science and Technology under contract YBKT09-05.

References

Barenblatt, G.I. (1959), “The formation of equilibrium cracks during brittle fracture: general ideas and hypothesis, axially symmetric cracks”, *Appl. Math. Mech*., **23**, 622-636.

Benzeggagh, M.L. and Kenane, M. (1996), “Measurement of mixed-mode delamination fracture toughness of unidirectional glass/epoxy composites with mixed mode bending apparatus”, *Compos. Sci. Technol.,* **56**, 439-449.

Brara, A. and Klepaczko, J.R. (2007), “Fracture energy of concrete at high loading rates in tension”, *Int. J. Impact. Eng*., **34**, 424-435.

Buyukozturk, O. and Hearing, B. (1998), “Crack propagation in concrete composites influenced by interface fracture parameters", *Int. J. Solids. Struct.,* **35**, 4055-4066.

Cai, M., Kaiser, P.K., Suorineni, F. and Su, K. (2007), "A study on the dynamic behavior of the Meuse/Haute-Marne argillite", *Phys. Chem. Earth*., **32**, 907-916.

Camacho, G.T. and Ortiz, M. (1996), "Computational modeling of impact damage in brittle materials", *Int. J. Solids. Struct.,* **33**, 2899-2938.

Cotsovos, D.M. and Pavlović, M.N. (2008), "Numerical investigation of concrete subjected to high rates of uniaxial tensile loading", *Int. J. Impact. Eng*., **35**, 319-335.

Cotsovos, D.M. and Pavlović, M.N. (2008), "Numerical investigation of concrete subjected to compressive impact loading. Part 1: A fundamental explanation for the apparent strength gain at high loading rates", *Comput. Struct*., **86**, 145-163.

Cotsovos, D.M. and Pavlović, M.N. (2008), "Numerical investigation of concrete subjected to compressive impact loading. Part 2: Parametric investigation of factors affecting behavior at high loading rates", *Comput. Struct*., **86**, 164-180.

Dugdale, D.C. (1960), "Yielding of steel sheets containing slits", *J. Mech. Phys. Solids*., **8**, 100-104.

Wei, X.Y. and Hao, H. (2009), "Numerical derivation of homogenized dynamic masonry material properties with strain rate effects", *Int. J. Impact. Eng*., **36**, 522-536.

Geubelle, P.H. and Baylor, J. (1998), "Impact-induced delamination of laminated composites: a 2D simulation", *Compos. Part B Eng*., **29**(5), 589-602.

He, M.Y. and Hutchinson, J.W. (1989), "Crack deflection at an interface between dissimilar elastic materials", *Int. J. Solids. Struct*., **25**, 1053-1067.

Klepaczko, J.R. and Brara, A. (2001), "An experimental method for dynamic tensile testing of concrete by spalling", *Int. J. Impact. Eng*., **25**, 387-409.

Liu, L.G., Ou, Z.C., Duan, Z.P. and Huang, F.L. (2010), "Strain-rate effects on deflection/penetration of crack terminating perpendicular to bimaterial interface under dynamic loadings", *Int. J. Fract*., **167**, 135-145.

Needleman, A. (1990a), "An analysis of tensile decohesion along an interface", *J. Mech. Phys. Solids*., **38**, 289-294.

Ou, Z.C., Duan, Z.P. and Huang, F.L. (2010), "Analytical approach to the strain rate effect on the dynamic tensile strength of brittle materials", *Int. J. Impact. Eng*., **37**, 942-945.

Qi, C.Z., Wang, M.Y. and Qian, Q.H. (2009), "Strain-rate effects on the strength and fragmentation size of rocks", *Int. J. Impact. Eng*., **36**, 1355-1364.

Rice, J.R. (1968), *Mathematical Analysis in the Mechanics of Fracture*, Ed. Liebowitz, H., Fracture, Vol 2, *Academic Press*, New York.

Rice, J.R. and Wang, J.S. (1989), "Embrittlement of interfaces by solute segregation", *Mater. Sci. Eng. A*., **107**, 23-40.

Siegmund, T., Fleck, N.A. and Needleman, A. (1997), "Dynamic crack growth across an interface", *Int. J. Fract*., **85**, 381-402.

Tvergaard, V. (1990), "Effect of fibre debonding in a whisker-reinforced metal", *Mater. Sci. Eng. A*., **125**(2), 203-213.

Tvergaard, V. and Hutchinson, J.W. (1992), "The relation between crack growth resistance and fracture process parameters in elastic-plastic solids", *J. Mech. Phy. Solids*., **40**(6), 1377-1397.

Weerheijm, J. and Van Doormaal, J.C.A.M. (2007), "Tensile failure of concrete at high loading rates New test data on strength and fracture energy from instrumented spalling tests", *Int. J. Impact. Eng*., **34**, 609-626.

Xu, X.P. and Needleman, A. (1993), "Void nucleation by inclusion debonding in a crystal matrix", *Model. Simul. Mater. Sci. Eng*., **1**(2), 111-132.

Zhang, Z.Y. and Paulino, G.H. (2005), "Cohesive zone modeling of dynamic failure in homogeneous and functionally graded materials", *Int. J. Plast*., **21**, 1195-1254.

Zhang, M.H., Shim, V.P.W., Lu, G. and Chew, C.W. (2005), "Resistance of high-strength concrete to projectile impact", *Int. J. Impact. Eng*., **31**, 825-841.